Taylor & Francis
Taylor & Francis Group

Vehicle System Dynamics
International Journal of Vehicle Mechanics and Mobility

ISSN: 0042-3114 (Print) 1744-5159 (Online) Journal homepage: http://www.tandfonline.com/loi/nvsd20

Evaluation of chassis control method through optimisation-based controllability region computation

Shinichiro Horiuchi

To cite this article: Shinichiro Horiuchi (2012) Evaluation of chassis control method through optimisation-based controllability region computation, Vehicle System Dynamics, 50:sup1, 19-31, DOI: 10.1080/00423114.2012.657653

To link to this article: https://doi.org/10.1080/00423114.2012.657653

Vehicle System Dynamics
Vol. 50, Supplement, 2012, 19–31

Taylor & Francis
Taylor & Francis Group

Evaluation of chassis control method through optimisation-based controllability region computation

Shinichiro Horiuchi*

Department of Mechanical Engineering, Nihon University, 1-8 Kanda Surugadai, Chiyoda-ku, Tokyo 101-8308, Japan

(*Received 3 November 2011; final version received 7 January 2012*)

This paper proposes a new systematic evaluation approach for vehicle maneuverability based on controllability region computations. In this approach, the controllability region, defined as the set of vehicle initial states that can be transferred to a stable equilibrium point in the state space by using allowable controls, is calculated. The size of the controllability region for an open-loop system can serve as a measure of the intrinsic performance of the control method, because if the vehicle state is displaced outside of the controllability region, no controller will be able to maintain vehicle stability. The problem of determining the controllability region boundary is formulated as an optimisation problem such that the controls maximising the norm of the initial state can be determined. Thereby, the performances of four-wheel steering control and direct yaw moment control are evaluated and compared by the proposed procedure.

Keywords: chassis control; controllability region; optimisation; evaluation

1. Introduction

Chassis control systems must be designed to ensure that intended functions are preformed under all foreseeable operating conditions. Critical to safety, these control systems require extensive validation prior to market entry. However, owing to the increased use of advanced control algorithms, validation of chassis control systems is becoming progressively more difficult. Car manufacturers are thus faced with this challenging task of validation, which is a lengthy and expensive process for highly complex chassis control systems. The validation process is an integrated procedure involving analytical and experimental methods. Before a vehicle is experimentally tested at the proving ground, the chassis control systems have to be analytically shown to be safe and reliable, and to have the desired performance under all possible operational conditions. Moreover, the analytical results assist in defining experimental evaluations that are to be performed in proving ground tests.

*Email: horiuchi@mech.cst.nihon-u.ac.jp

ISSN 0042-3114 print/ISSN 1744-5159 online

http://dx.doi.org/10.1080/00423114.2012.657653
http://www.tandfonline.com

Analytical validation methods include robustness analysis [1], worst-case analysis [2,3], bifurcation analysis [4], and controllability analysis. Among these analytical methods, controllability analysis rooted in the computation of the controllability region is central to the problem of establishing that a system is safe. The controllability region is defined as the set of initial conditions that can be controlled to an equilibrium point by means of admissible controls. The size of the controllability region for an open-loop system can serve as a measure of the intrinsic performance of the *control method*, because if external disturbances move the system out of the controllability region, no controller will be able to maintain system stability. In this paper, a *control method* denotes the input channels used to control the vehicle motion, regardless of which control algorithm is used to generate the control inputs. For example, four-wheel steering (4WS) control uses front and rear steer angles as control inputs, whereas direct yaw moment control (DYC) uses front steer angle and torques applied to each wheel as control inputs. Closed-loop chassis control algorithms are designed by using given input channels to satisfy control objectives, such as improvement in stability, model following, and robustness. Existing research has not distinguished between open-loop control methods and closed-loop control algorithms, as a result, identification of the factors that limit the performance of each control system is not possible.

Although a number of studies on controllability analysis have been reported in flight dynamics and control [5–7], articles on the application of controllability analysis to chassis control systems do not appear to have been published to date. Therefore, this paper shows the results of a controllability region analysis of chassis control methods based on an optimisation approach. This approach allows us to clarify the performance limitations of a *control method*, independent of the control algorithm used. This work makes the following contributions. First, a method is proposed to compute the controllability region based on the optimisation approach. Second, a comparison is given between the performance limits of certain control methods by determining the size of the controllability region. Finally, the proposed approach is shown to be a viable analytical method in the validation process of chassis control systems.

The remainder of this paper is organised as follows. In Section 2, controllability fundamentals and computation of the controllability region are briefly described. Sections 3 and 4 outline the vehicle model and the control methods considered in this study, respectively. Results of controllability region computations and comparisons between the methods are given in Section 5. Finally, concluding remarks appear in Section 6.

2. Controllability region

2.1. *Definition of controllability region*

Consider the general nonlinear system

$$\dot{\boldsymbol{x}} = \boldsymbol{f}(\boldsymbol{x}, \boldsymbol{u}, t), \quad t_0 \geq t \geq \tau, \quad \boldsymbol{x}(t_0) = \boldsymbol{x}_0, \tag{1}$$

where $\boldsymbol{x} \in \mathbb{R}^n$ is the state vector and $\boldsymbol{u} \in \mathbb{R}^m$ is the control vector. The function $\boldsymbol{f}(\boldsymbol{x}, \boldsymbol{u}, t)$ is assumed to be continuously differentiable in $\boldsymbol{x}$, $\boldsymbol{u}$, t for all $t \geq t_0$ and all $\boldsymbol{x} \in \mathbb{R}^n$, $\boldsymbol{u} \in \mathbb{R}^m$. For a specified target set, $\mathcal{X}$, and control constraint

$$\boldsymbol{u}_{\min} \leq \boldsymbol{u}(t) \leq \boldsymbol{u}_{\max}, \tag{2}$$

where the inequalities are treated component-wise, the controllable set $\mathcal{C}(\tau, t_0, \boldsymbol{x}_0) \in \mathbb{R}^n$ to the target set $\mathcal{X}$ at time $\tau > t_0$ is defined as the set of all initial states that can be transferred

to the target by using a subset of the admissible controls [8]. For a linear time-invariant system without input constraints, the controllable set is the entire state space if the system is controllable. However, in general, a nonlinear system has a restricted controllable set around the target. From a graphical viewpoint, the controllable set is referred to as the *controllability region*. The controllability region is a useful design tool for comparing the effectiveness of different control methods.

2.2. *Computation of controllability region*

Determination of the controllability region for a linear system under input saturation has been widely studied and a number of computational techniques have been proposed [9–11]. However, computation of the exact controllability region for a nonlinear continuous time system is in general a highly nontrivial task, especially for multidimensional systems. The controllability region boundary of low-dimensional nonlinear systems may be found by directly applying the controllability minimum principle [12]. However, use of the controllability minimum principle in determining the controllability region is limited to problems of three dimensions or less. Therefore, one approach to establish the multidimensional controllability region is to consider the projected controllability region, that is, projection of a high-dimensional controllability region onto a region with lower dimension [13].

In this paper, we assume that the multidimensional controllability region can be analysed by a number of two-dimensional cross sections. Different combinations of these cross sections then help to visualise the multidimensional region. This analogue problem significantly simplifies the computation of the controllability region. Note that comparisons of the cross sections give us necessary, but not sufficient, conditions for evaluation of the control method: proximity of specific cross sections in different control methods does not guarantee the closeness of cross sections in all orientations. Nevertheless, this cross-section method provides useful information on the controllability region.

Computation of the two-dimensional cross sections of the controllability region can be achieved by a grid point method, where a fine grid is defined on a cross section and each grid point is assumed to be an initial condition of the state equation. Next, a two-point boundary value problem, in which numerical integration begins at each grid points and ends at $\mathcal{X}$, is solved. Grid points are thus classified according to the results of integration: if control inputs exist that take the trajectory from a grid point to $\mathcal{X}$, then the grid point is controllable, otherwise the point is uncontrollable. This approach is simple, but time consuming. Therefore, in this paper, we propose an optimisation-based method combined with the ray-gridding technique [14] for computing the controllability region.

2.3. *Optimisation-based controllability region computation*

The problem of finding the controllability region boundary, $\partial\mathcal{C}$, can be formulated as an optimal control problem that maximise the norm of the initial condition $\boldsymbol{x}_0$ on the cross section with terminal constraint $\boldsymbol{x}(\tau) \in \mathcal{X}$. Instead of standard gridding, the ray-gridding technique operates in terms of rays. Let us consider a set of rays $r_k, k = 1, 2, \ldots$ radiating in different directions from the centre of the x_i–x_j cross section, as shown in Figure 1. Here, the angle defining the direction of the kth ray is denoted as θ_k. By assuming that the controllability region is convex, the point of intersection between $\partial\mathcal{C}$ and r_k is the solution of the following optimal control problem.

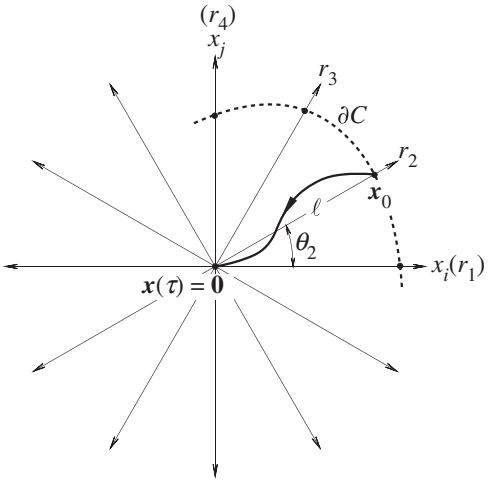

Figure 1. Ray-gridding method.

Find control vector $\boldsymbol{u}(t), t \in [t_0, \tau]$ that maximises

$$J = \ell = \|\boldsymbol{x}_0\| \tag{3}$$

subject to

$$x_i(0) = \ell \cos\theta_k, \quad x_j(0) = \ell \sin\theta_k, \tag{4}$$

$$x_i(\tau) = 0, \quad x_j(\tau) = 0, \tag{5}$$

and the additional terminal constraint

$$\boldsymbol{\psi}\{\boldsymbol{x}(\tau)\} = \boldsymbol{0}, \tag{6}$$

where $\mathcal{X}$ is assumed to be the origin of the x_i–x_j cross section.

Solution of this optimal control problem can be obtained using a modified version of the minimum principle that properly accounts for both the control and state constraints. However, because of the computational demand in the application of the minimum principle, here the simple transcription method [15] is employed that is based on discrete approximation of the control input. In the transcription method, the optimal control problem is transformed into a parameter optimisation problem and is solved by an existing nonlinear programming code. The primary advantage of this method is that it can easily handle general problems that involve constraints such as those in Equations (2), (5), and (6).

The control input, $\boldsymbol{u}(t)$, is parameterised by dividing the time interval of the optimal control problem, $[t_0, \tau]$, into N subintervals:

$$t_0 < t_1 < \cdots < t_{N-1} < t_N = \tau. \tag{7}$$

Typically, these subintervals are of equal size. Thus, the continuous function of time $\boldsymbol{u}(t)$ is replaced with its discrete values, $\boldsymbol{u}_m$, at $t_m, m = 0, 1, \ldots, N$. The unknowns of the parameter optimisation problem are then the norm of the initial state, ℓ, and the discretised controls, $\boldsymbol{u}_m$. We now suppose that ℓ and $\boldsymbol{u}_m$ are given and placed in an unknown parameter vector $\boldsymbol{X}$,

$$\boldsymbol{X} = [\ell \ \boldsymbol{u}_0^T \ \boldsymbol{u}_1^T \ \cdots \ \boldsymbol{u}_N^T], \tag{8}$$

which contains $1 + m(N + 1)$ elements. With $\boldsymbol{X}$ generated, the state equation, Equation (1), can be integrated numerically from $t = t_0$ to τ to obtain the states at $t_m, m = 0, 1, \ldots, N$. During this integration, the controls are assumed to change linearly between time intervals. As a result of integration, the states at t_m, denoted $\boldsymbol{x}_m$, become functions of only the parameter vector $\boldsymbol{X}$:

$$\boldsymbol{x}_m = \boldsymbol{x}_m(\boldsymbol{X}). \tag{9}$$

Similarly, the equality constraints in Equations (5) and (6) and the inequality constraints in Equation (2) become functions of $\boldsymbol{X}$. Moreover, the performance function in Equation (3) can be rewritten as

$$J = J(\boldsymbol{X}). \tag{10}$$

Hence, the optimal control problem can be reduced to the following parameter optimisation problem.

Find $\boldsymbol{X}$ that maximises

$$J = J(\boldsymbol{X}) \tag{11}$$

subject to

$$\boldsymbol{x}'(0) = \boldsymbol{x}'_0(\boldsymbol{X}), \tag{12}$$

$$\boldsymbol{x}'(t_N) = \boldsymbol{0}, \tag{13}$$

$$\boldsymbol{\psi}\{\boldsymbol{x}(\boldsymbol{X})\} = \boldsymbol{0}, \tag{14}$$

where $\boldsymbol{x}' = [x_i\ x_j]^{\mathrm{T}}$. This parameter optimisation problem can be solved by mathematical programming techniques, such as sequential quadratic programming. To increase the possibility that the global optimum is found, rather than being trapped at a local maximum, a multistart technique [16] is utilised, in which a number of initial input profiles are supplied to the search algorithm.

3. Vehicle modelling

3.1. *Vehicle model*

The vehicle model used in this paper involves longitudinal, lateral, directional, and sprung-mass roll degrees-of-freedom, and includes a spin mode for each wheel [17]. From Figure 2, the equations of motion describing the basic degrees-of-freedom are derived as

$$\text{Longitudinal motion: } m(\dot{u} - rv) = F_x; \tag{15}$$

$$\text{Lateral motion: } m(\dot{v} + ur) + m_s h_s \dot{p} = F_y; \tag{16}$$

$$\text{Yaw motion: } I_{zz}\dot{r} - I_{xz}\dot{p} = N; \tag{17}$$

$$\text{Roll motion: } I_{\phi}\dot{p} - I_{xz}\dot{r} + m_s h_s(\dot{v} + ur) = L_s. \tag{18}$$

Here, h_s is the distance between the centre of the sprung mass and the roll axis, I_{ϕ} is the moment of inertia about roll axis, and m_s is the sprung mass. External forces F_x and F_y along

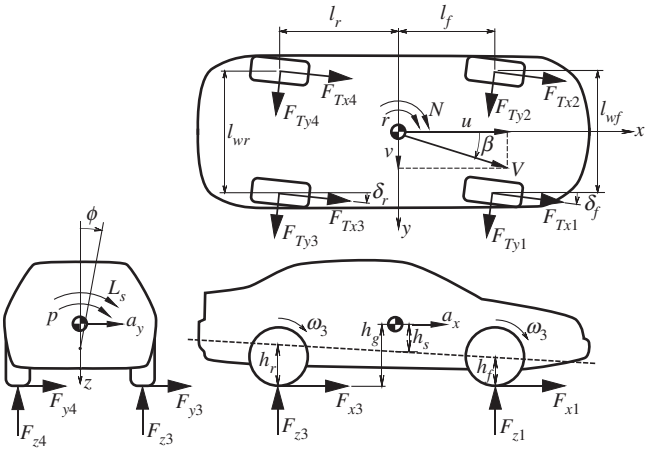

Figure 2. Schematic of vehicle model.

the x and y axes of the vehicle and moment N are assumed to result exclusively from the friction force between the tyres and road:

$$F_x = \sum_{i=1}^{4} F_{xi}, \tag{19}$$

$$F_y = \sum_{i=1}^{4} F_{yi}, \tag{20}$$

$$N = \frac{l_{wf}}{2}(-F_{x1} + F_{x2}) + l_f(F_{y1} + F_{y2}) + \frac{l_{wr}}{2}(-F_{x3} + F_{x4}) - l_r(F_{y3} + F_{y4}). \tag{21}$$

Since tyre forces, F_T, are defined in the wheel axis coordinate system, F_T must be rewritten in terms of vehicle axis coordinates:

$$F_{x(1,2)} = F_{Tx(1,2)} \cos\delta_f - F_{Ty(1,2)} \sin\delta_f, \tag{22}$$

$$F_{y(1,2)} = F_{Tx(1,2)} \sin\delta_f + F_{Ty(1,2)} \cos\delta_f, \tag{23}$$

$$F_{x(3,4)} = F_{Tx(3,4)} \cos\delta_r - F_{Ty(3,4)} \sin\delta_r, \tag{24}$$

$$F_{y(3,4)} = F_{Tx(3,4)} \sin\delta_r + F_{Ty(3,4)} \cos\delta_r. \tag{25}$$

Rolling moments are provided by the springs and shock absorbers:

$$L_s = (m_s g h_s + G_\phi)\phi + C_\phi p, \tag{26}$$

where G_ϕ is the roll stiffness and C_ϕ is the roll damping.

The tyre forces result from the tyre lateral slip angle, longitudinal slip ratio, camber angle, and normal load. The sideslip angles of the tyres have components resulting from body velocities and wheel deflections due to steering input, roll steer, and compliance steer. The transfer of normal load on each wheel from cornering, acceleration, and braking is a critical aspect of vehicle dynamics and contribute to limiting a vehicle's maneuvering ability. Here, normal loads are assumed to be a function of the vehicle's weight, mg, longitudinal acceleration, a_x,

lateral acceleration, a_y, and front/rear axle roll stiffness distributions, G_f^*, G_r^*:

$$F_{z1} = \frac{l_r}{2l}mg - \frac{ma_x h_g}{2l} - \frac{1}{l_{wf}}\left\{G_f^*(ma_y + m_s g\phi)h_s + \frac{l_r}{l}ma_y h_f\right\}, \tag{27}$$

$$F_{z2} = \frac{l_r}{2l}mg - \frac{ma_x h_g}{2l} + \frac{1}{l_{wf}}\left\{G_f^*(ma_y + m_s g\phi)h_s + \frac{l_r}{l}ma_y h_f\right\}, \tag{28}$$

$$F_{z3} = \frac{l_f}{2l}mg + \frac{ma_x h_g}{2l} - \frac{1}{l_{wr}}\left\{G_r^*(ma_y + m_s g\phi)h_s + \frac{l_f}{l}ma_y h_r\right\}, \tag{29}$$

$$F_{z4} = \frac{l_f}{2l}mg + \frac{ma_x h_g}{2l} + \frac{1}{l_{wr}}\left\{G_r^*(ma_y + m_s g\phi)h_s + \frac{l_f}{l}ma_y h_r\right\}, \tag{30}$$

where h_f and h_r denote the heights of the front and rear roll centres, respectively.

3.2. *Tyre model*

The tyre model used in this study [18] requires tyre lateral slip angle, β_i, longitudinal slip, s_i, normal load, F_{z_i}, and camber angle, γ_i as inputs, and generates lateral tyre force, F_{Ty_i}, and longitudinal tyre force, F_{Tx_i} as outputs to the vehicle dynamics model:

$$F_{Ty_i} = \mu_{0_i} F_{z_i}\left(\frac{f(\sigma_i)K_{s_i}\tan\beta_i}{\sqrt{K_{s_i}^2\tan^2\beta_i + K_{c_i}^2 s_i^2}} + Y_{\gamma_i}\gamma_i\right), \tag{31}$$

$$F_{Tx_i} = \mu_{0_i} F_{z_i}\frac{f(\sigma_i)K_{c_i}s_i}{\sqrt{K_{s_i}^2\tan^2\beta_i + K_{c_i}^2 s_i^2}}, \tag{32}$$

where f is the force saturation function, which is a function of composite slip σ_i. The composite slip is in turn a function of β_i, s_i, and load-dependent longitudinal and lateral stiffness coefficients K_{c_i} and K_{s_i}. Here, Y_γ is the load-varying camber thrust coefficient.

Figure 3 shows the typical tyre force characteristics under a zero camber angle. Force reduction is apparent at high slip angles and at high longitudinal slip ratio levels. The interaction between the longitudinal and lateral forces is apparent in the figure. The tyre model response characteristics illustrated in Figure 3 clearly includes the full operating range of the tyre motion. A dynamic delay in the generation of the tyre's side force is approximated by a first-order lag system whose lag time constant is a function of the transition length and wheel speed.

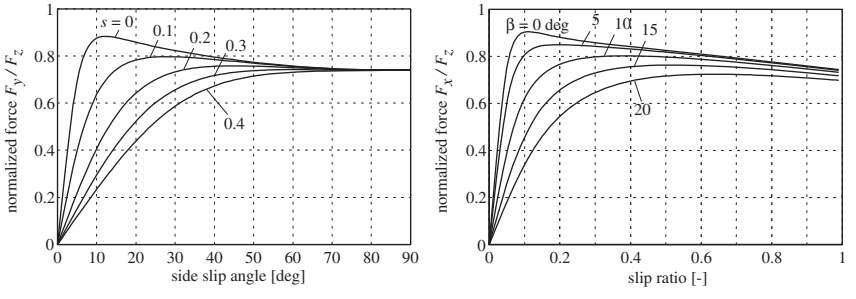

Figure 3. Tyre force response.

4. Control methods

Six control inputs are regarded as inputs to the vehicle model: front steering angle command, u_f; rear steering angle command, u_r; and braking torque commands, T_1–T_4. The following three control methods having different combination of these inputs are then considered in order to compare the inherent performance of the control method.

(1) *Conventional front wheel steering* In this case, only the front steering angle is considered as control input. Therefore, the control vector in Equation (1) is

$$\boldsymbol{u} = [u_f], \quad -u_{f_{\max}} \leq u_f \leq u_{f_{\max}}. \tag{33}$$

Inputs u_r and T_1–T_4, are held constant at zero.

(2) *Four-wheel steering* In addition to the front steering angle, the rear steering angle, u_r, is included in the control vector as

$$\boldsymbol{u} = [u_f \; u_r]^{\mathrm{T}}, \quad -u_{f_{\max}} \leq u_f \leq u_{f_{\max}}, \quad -u_{r_{\max}} \leq u_r \leq u_{r_{\max}}. \tag{34}$$

The braking torques on each wheel are assumed to be zero.

(3) *Direct yaw moment control* In addition to the front steering angle, braking torques on each wheel are included in the control input. A differential-braking torque gives an alternative means to control the yaw moment. For a given longitudinal acceleration limit, a, the required total braking force is calculated as ma. To generate this total force, torques on each wheel are determined by following equations:

$$\begin{aligned} T_1 &= Rmad_{fr}d_f, \quad 0 \leq a \leq a_{\max}, \\ T_2 &= Rmad_{fr}(1 - d_f), \quad 0 \leq d_{fr} \leq 1, \\ T_3 &= Rma(1 - d_{fr})d_r, \quad 0 \leq d_f \leq 1, \\ T_4 &= Rma(1 - d_{fr})(1 - d_r), \quad 0 \leq d_r \leq 1, \end{aligned} \tag{35}$$

where R is an effective tyre radius, d_{fr} is a front-to-rear torque distribution ratio, and d_f and d_r are the right to left torque distribution ratios for the front and rear wheels, respectively. Therefore, $\boldsymbol{u}$ for this case is

$$\boldsymbol{u} = [u_f \; a \; d_{fr} \; d_f \; d_r]^{\mathrm{T}}. \tag{36}$$

The rear steering angle is fixed at zero.

5. Computational conditions

According to the theoretical definition of the controllability region, the size of the region is dependent on the time taken to transfer the state from the set of initial conditions to the target set $\mathcal{X}$. From a practical viewpoint, a long transition time is undesirable. Thus, the following constraint for terminal time, τ, is considered:

$$\tau \leq 1 \text{ s}. \tag{37}$$

With the number of subintervals for the time discretisation in Equation (7) set at 10, the optimal control inputs are calculated every 0.1 s.

Among the vehicle states described in Equation (1), the vehicle lateral/directional motion and stability are best described through the lateral velocity, v, and yaw rate, r. Therefore,

the v–r cross section is selected for calculation of the controllability region. Other than these two parameters, the initial conditions are assumed to be the same as those when running in a straight line. The total velocity, V, at t_0 is assumed to be 30 m/s.

The target set, $\mathcal{X}(v, r)$, of the controllability region is set as:

$$v(\tau) = 0, \quad r(\tau) = 0, \tag{38}$$

and the additional terminal constraint in Equation (6) is

$$\dot{v}(\tau) = 0, \quad \dot{r}(\tau) = 0. \tag{39}$$

This target set and terminal constraint are chosen such that the vehicle returns to straight-line running.

6. Results of the controllability region computation

6.1. *Front wheel steering*

Figure 4 shows the controllability region of a 2WS vehicle when the limit of the front steering command $u_{f_{\max}} = 5°$. As indicated in this figure, the controllability region spreads towards the first and third quadrants of the v–r cross section. For the readers' interest, a number of trajectories starting from the $\partial\mathcal{C}$ boundary are superimposed onto this figure. The optimal front steering angle ensures convergence of all trajectories towards the target set $\mathcal{X}$. Note that the paths of certain trajectories cross the plane, since the plane is a cross section of the multidimensional phase space.

Figure 5 illustrates three examples of the optimal front steering angle, lateral velocity, and yaw rate at the points marked in Figure 4. The optimal controls satisfy the constraints for upper and lower boundaries. From Figure 4, discontinuities in the controllability region boundary exist in the first and third quadrants. For trajectories originating at either side of these discontinuity points, changes are observed in the pattern of the optimal control as shown in Figure 5.

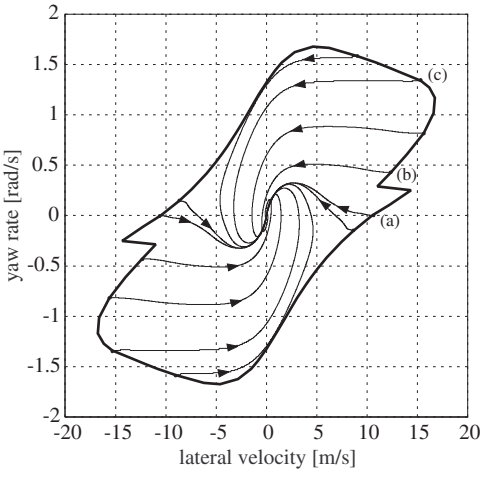

Figure 4. v–r controllability region cross section of front wheel steering (2WS) vehicle, $u_{f_{\max}} = 5°$, $\tau = 1.0$ s.

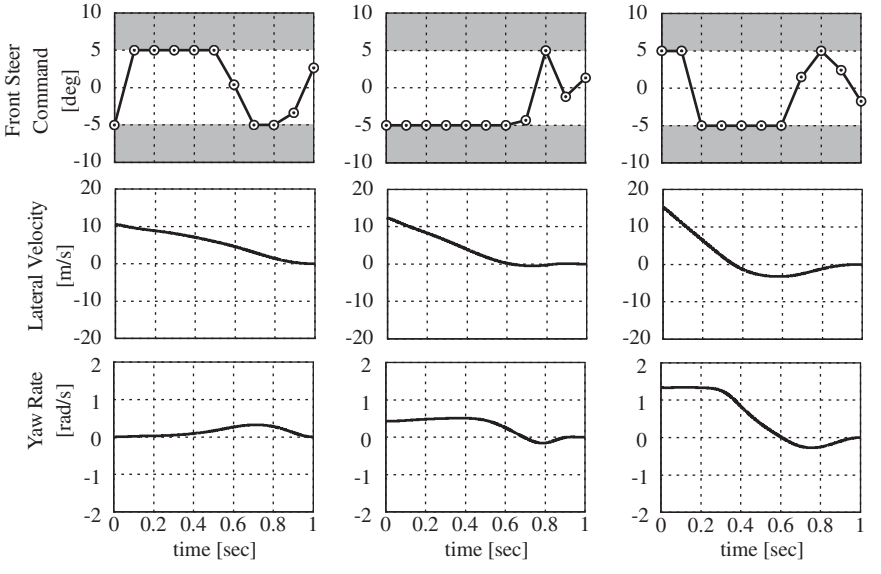

Figure 5. Optimal front steering angle, lateral velocity, and yaw rate at the corresponding points in Figure 4.

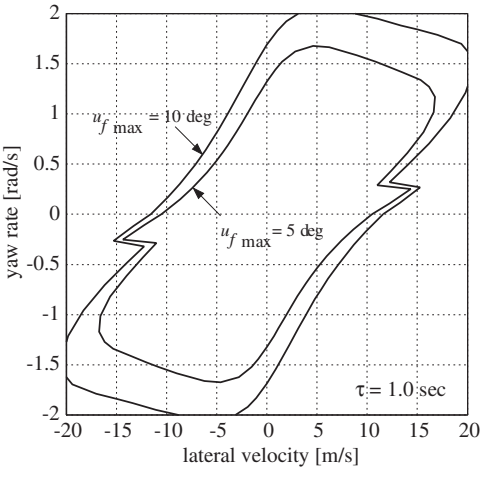

Figure 6. Effect of increasing maximum front steer angle, $\tau = 1.0$ s.

6.2. *2WS, effect of maximum steer angle*

Figure 6 shows the effect of maximum front steering angle on the size of the controllability region. As expected, a large front steering angle results in a larger controllability region. This expansion effect is particularly apparent in the first and the third quadrants compared with the second and fourth quadrants.

6.3. *2WS, effect of transition time*

Figure 7 illustrates the effect of varying the transition time, τ. The controllability regions for three different transition times are computed and compared, and a short transition time results in smaller controllability region.

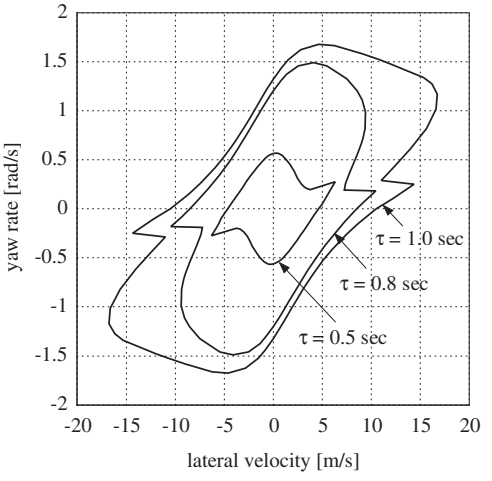

Figure 7. Effect of terminal time, $u_{f_{\max}} = 5°$.

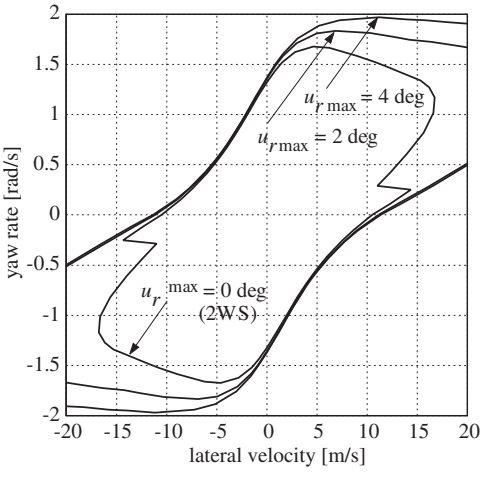

Figure 8. v–r controllability region cross section for 4WS vehicle, $u_{f_{\max}} = 5°$.

6.4. *Four-wheel steering*

The result of adding rear wheel steering to the vehicle on the size of the controllability region is shown in Figure 8. As seen in Figure 6 for the 2WS case, a large rear steering angle expands the controllability region, especially in the first and third quadrants. In the second and fourth quadrants, an increase in limit of the rear steering angle has no effect on the size of the controllability region. Because the lateral forces of rear tyres are saturated in second and fourth quadrants, additional rear steering does not enlarge the controllability region in these quadrants.

6.5. *Direct yaw moment control*

The effect of DYC, specifically, the effect of differential braking, on the size of the controllability region is shown in Figure 9. In contrast to the 4WS case, a large torque increases

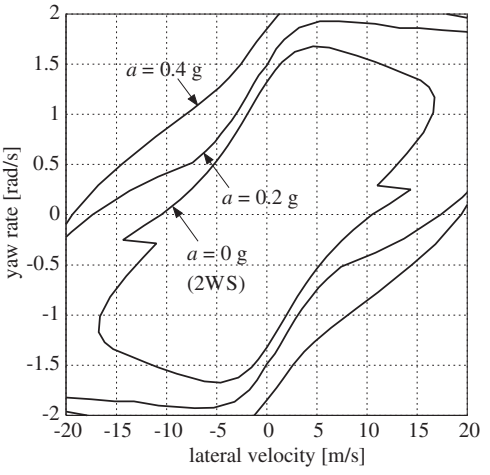

Figure 9. v–r controllability region cross section for DYC vehicle, $u_{f_{\max}} = 5°$.

the controllability region not only in the first and third quadrants, but also in the second and fourth quadrants. Therefore, if the vehicle states v and r are perturbed to either the second or fourth quadrant, DYC has the ability to return the vehicle to the original straight-line running condition. This result shows the advantage of the DYC control method over 4WS. We conclude that no amount of design will enable the 4WS controller to exceed the performance of the DYC.

7. Conclusion

This paper has presented an evaluation of chassis control methods by computing the controllability region of each method. An optimisation-based method was proposed for this computation. As a result, the controllability regions of three control methods were calculated by the proposed method: conventional 2WS, 4WS, and DYC. The effects of the maximum steering angle and the transition time on the size of the controllability region were examined. From a comparison of the calculated controllability regions, the advantage of using DYC above 4WS as a vehicle control method was demonstrated.

Acknowledgements

This research was partially supported by Japan Society for the Promotion of Science, Grant-in-Aid for Scientific Research No. 21560250. The author thanks Mr. K. Amemiya from Honda R&D Co. Ltd. for his cooperation in the numerical computations, and Mr. K. Okada from Honda R&D Co. Ltd. for his valuable comments.

References

[1] S. Horiuchi, K. Okada, and S. Nohtomi, *Stochastic robustness analysis and synthesis of nonlinear vehicle dynamics controller*, Veh. Syst. Dyn. 37(suppl.) (2001), pp. 183–196.
[2] W. Ma and H. Peng, *A worst-case evaluation method for dynamic systems*, J. Dyn. Syst. Meas. Control 121(2) (1999), pp. 191–199.
[3] K. Amemiya and S. Horiuchi, *Bounded-input bounded-output stability analysis of vehicles using worst-case input*, Rev. Autom. Eng. 26(2) (2005), pp. 177–184.

[4] K. Okada, S. Nohtomi, and S. Horiuchi, *Assessment of Chassis Control Systems Using Constrained Bifurcation and Continuation Method*, Proceedings of the 9th International Symposium on Advanced Vehicle Control (AVEC 2008), Kobe, Japan, 6–9 October 2008, pp. 585–597.
[5] M.G. Goman and M.N. Demenkov, *Computation of controllability regions for unstable aircraft dynamics*, J. Guid. Control Dyn. 27(4) (2004), pp. 647–656.
[6] A.M. Bayen and C.J. Tomlin, *Aircraft autolander safety analysis through optimal control-based reach set computation*, J. Guid. Control Dyn. 30(1) (2007), pp. 68–77.
[7] R. Pandita, A. Chakraborty, P. Seiler, and G. Balas, *Reachability and Region of Attraction Analysis applied to GTM Dynamic Flight Envelope Assessment*, AIAA paper 2009-6258, American Institute of Aeronautics and Astronautics, Reston, VA, 2009.
[8] T.L. Vincent and W.J. Grantham, *Nonlinear and Optimal Control Systems*, Chap. 6, Wiley, New York, 1997.
[9] A.M. Formal'skii, *Controllability domain of systems having limited control resources*, Autom. Remote Control 29(3) (1968), pp. 375–382.
[10] T. Hu and Z. Lin, *Control System with Actuator Saturation: Analysis and Design*, Chap. 2, Birkhauser, Basel, 2001.
[11] W.L.A. Wang and Y.J. Chen, *3D controllable set of linear time-invariant open-loop unstable systems with constrained input – a submarine case*, Eng. Lett. 16(2) (2008), pp. 185–192.
[12] W.J. Grantham and T.L. Vincent, *A controllability minimum principle*, J. Optim. Theory Appl. 17(1–2) (1975), pp. 93–114.
[13] T.L. Vincent and Z.Y. Wu, *Estimating projections of the controllable set*, J. Guid. Control Dyn. 13(3) (1990), pp. 572–575.
[14] C.A. Yfoulis, A. Muir, and P.E. Wellstead, *A new approach for estimating controllable and recoverable regions for systems with state and control constraints*, Int. J. Robust Nonlinear Control 12 (2002), pp. 561–589.
[15] J.T. Betts, *Practical Methods for Optimal Control Using Nonlinear Programming*, SIAM, Philadelphia, PA, 2001.
[16] Z.B. Zabinsky, *Stochastic Adaptive Search for Global Optimization*, Kluwer Academic, Dordrecht, 2003.
[17] R.W. Allen, H.T. Szostak, T.J. Rosenthal, and D.E. Johnson, *Test Methods and Computer Modeling for the Analysis of Ground Vehicle Handling*, SAE 861115, SAE international, Warrendale, PA, 1986.
[18] R.W. Allen, T.J. Rosenthal, and H.T. Szostak, *Steady-State and Transient Analysis of Ground Vehicle Handling*, SAE 870495, SAE international, Warrendale, PA, 1987.